Getting more early photons with less background: detection rate and signal-to-background improvements in enhanced early photon imaging

Lagnojita Sinha, Jovan G. Brankov, Kenneth M. Tichauer

Lagnojita Sinha, Jovan G. Brankov, Kenneth M. Tichauer, "Getting more early photons with less background: detection rate and signal-to-background improvements in enhanced early photon imaging," Proc. SPIE 10486, Design and Quality for Biomedical Technologies XI, 104860E (19 February 2018); doi: 10.1117/12.2287182

SPIE.

Event: SPIE BiOS, 2018, San Francisco, California, United States

Getting more early photons with less background: detection rate and signal-to-background improvements in enhanced early photon imaging

Lagnojita Sinha*[a], Jovan G. Brankov [b], Kenneth M. Tichauer[a]

[a]Biomedical Engineering, Illinois Institute of Technology, Chicago, IL 60616, USA; [b]BElectrical and Computer Illinois Institute of Technology, Chicago, IL 60616

ABSTRACT

With tissue samples less than 1 mm in thickness, optical projection tomography (OPT) has proven to be a very powerful imaging modality that can achieve high spatial resolution images. This high resolution is achieved by collecting the photons with non-significant scattering through 1 mm of tissue, the so-called diffusion limit. But, with samples thicker than 1 mm, scattered photons dominate and the highly resolved images give way to significantly "blurred" images in OPT[1]. However, as increased scattering relates to increased time of travel of the photons so time-domain OPT has been used to only collect the early-arriving photons that have travelled a more direct route through the tissue to reduce detection of scattered photons. Yet very early photons are extremely rare compared to scattered photons. Our recent suggested early photon count rates can be significantly enhanced by running the detector in a "deadtime" regime where the deadtime incurred by early-arriving photons acts as a shutter to later-arriving scattered photons[2]. In this work, we will demonstrate that running in the deadtime also had the unexpected advantage of significantly reducing the number of background photons detected. Proposed approach increases the early photon detection rate by 3-orders-of-magnitude in comparison with conventional approaches in 4-mm thick tissues with 780 nm light while the laser power is far below the level that would significantly damage the tissue. In addition, the signal to background (caused by after pulsing) was improved by 70-fold compared to conventional approaches designed to collect an equal number of early photons.

Keywords: enhanced early photon imaging, SPAD, Monte Carlo simulation

1. INTRODUCTION

One of the leading causes of cancer death among females is breast cancer that accounts for 14% of total cancer death[3]. Metastasis in breast cancer is detected by sentinel lymph node (tumor draining lymph node) biopsy after it is surgically resected– a critical step for the selection of future therapy[4, 5]. While pathology can determine microscopic cancer spreads in the lymph node it would require prohibitive tissue processing time. So, current practice is to analyze the node every 2 mm and this can miss microscopic tumor burden (micro-metastasis) if they are < 2 mm[6]. Therefore an ultimate objective would be to develop an imaging system in the mesoscopic domain (1 mm - 1 cm) that can rapidly and non-destructively map microscopic tumor burden in excised lymph nodes and therefore guide pathology accordingly to give more accurate results.

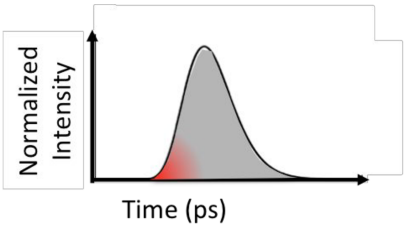

Figure 1. The pulse spread function that exits from the tissue has rare early arriving photons (red regon) which gives way to more scattered late arriving photons (grey region).

Optical imaging is a potential alternative to perform high-resolution imaging without any harmful effect of radiation (like x-ray computed tomography, single photon emission computed tomography or positron emission tomography) but it is limited by the high amount of scattering in tissue[7]. High resolution images (<1 μm) are obtained in microscopy for thin slices of tissue (<<1 mm) but the resolution drops exponentially with increased tissue thickness (Diffused optical tomography has a resolution ~mm for >1 cm thick tissue[8]). This is due to the scattering phenomenon in tissue that bars the ability to predict the original photon path for tissue thicker than 1 mm[9]. In optical imaging since scattered light is the main concern that causes blurriness in the image – few approaches have been implemented to remove these scattered photons to improve resolution (*e.g.*, through detection of the earliest arriving photons[10-13], implementing angular restriction[14], etc.). In case of time

Design and Quality for Biomedical Technologies XI, edited by Ramesh Raghavachari, Rongguang Liang, Proc. of SPIE Vol. 10486, 104860E · © 2018 SPIE · CCC code: 1605-7422/18/$18 · doi: 10.1117/12.2287182

domain restriction the arrival time of the photons are used to reject the scattered photons. **Fig. 1** shows the spreading of an instantaneous pulse after it has travelled through the tissue, also known as the temporal pulse spread function (TPSF). The photons that suffer minimum scatter in the tissue will remain near the principal axis, along the line of excitation by the source, and therefore will arrive earlier at the detector (marked with red in **Fig. 1**) compared to the ones which get scattered and therefore travels a larger path and reaches the detector at a later time point (marked with gray in **Fig. 1**). Since these scattered photons cause image domain blur, time domain restriction is used to reject these and therefore achieve a much higher resolution in optical imaging.

Our group has recently developed a method to further enhance the collection of early arriving photons by saturating the detector[2]. Once a single photon detector (e.g. single photon avalanche diode) detects a photon there is a lag time, which it takes to reset itself to detect the next photon. This is known as the dead time of the detector during which it does not detect any incoming photon. Since the detector always sees the first arriving photon and then goes into the dead time, if the laser pulse period is longer than the detector dead time then the early photons will get detected although we will lose the late arriving scattered photons as the detector then goes into its dead time. This approach of saturating the detector and utilizing most of its dynamic range to observe the very rare early photons and reject the scattered ones is used in performing enhanced early photon imaging. . Further since the "background" signal mainly constitutes of the afterpulsing signal by saturating the detector the background signal also gets saturated. Afterpulsing is a phenomenon in which a false signal is detected at the detector due to presence of residual charge after the true signal is generated and it is proportional to the number of detected photons, so when the detector is saturated - the true signal is saturated and hence the afterpulsing signal is also saturated. So, on one hand the early photon detection rate is increased by few orders of magnitude by saturating the detector and on the other hand the background signal is lesser compared to conventional mode. The novel discussion in this paper entails Monte Carlo simulation of the propagation of the Gaussian beam through the tissue and the discussion on the two-fold improvement in signal to background ratio by running the detector in dead-time mode.

2. METHODS

2.1 Experimental setup

The system used for enhanced early photon imaging application is presented in **Fig. 2**. The system is composed of a 780 – nm, 10-MHz, 12-mW femtosecond pulsed laser (Mendocino, Calmar Laser, Palo Alto, CA) having a <90 fs FWHM. A laser driver module drove the laser source. The light emitted from the source was passed through a band pass filter (ZET785/10x, Chroma Technology, Bellow Falls, VT), acting as a laser clean up filter and then through a motorized neutral density variable attenuator wheel (Thorlabs, Newton, NJ), which was manipulated to regulate the power hitting the sample. The laser light was then focused, through an aspheric doublet lens having a focal length of 75 mm (Thorlabs, Newton, NJ), to a sub-50-µm spot size on the surface of the sample holder (which is designed to contain the sample). A motorized stage assembly having three degrees of freedom is used to control the horizontal, vertical and rotational movement of the sample holder. Two similar 100mm focal length aspheric doublet lens was used on the other side of the sample holder at the opposite end of the source, acting as a collimator pair, to perform a 1:1 mapping of the 50-µm spot size on the back of the sample holder onto the detector i.e. focus light from a 50-µm spot size at the back of the detector to the 50-µm single photon avalanche diode – SPAD (50-µm PDM Series, MPD via PicoQuant, Berlin, Germany) used as our detector. The dead time of the detector is 77 ns. The detection signal from the SPAD was fed to the time correlated single photon counting (TCSPC) module (HydraHarp, PicoQuant) that also receives a synchronization signal from the laser driver module. The TCSPC module then performs time stamping of the arriving photons, generates the histogram of the arrival time of the photons and sends it to the computer which is then analyzed. The full width at half max (FWHM) of the instrument response function of the system was 35 ps. All automated components of the system were controlled by in-house software developed in Matlab (Mathworks, Natick, MA).

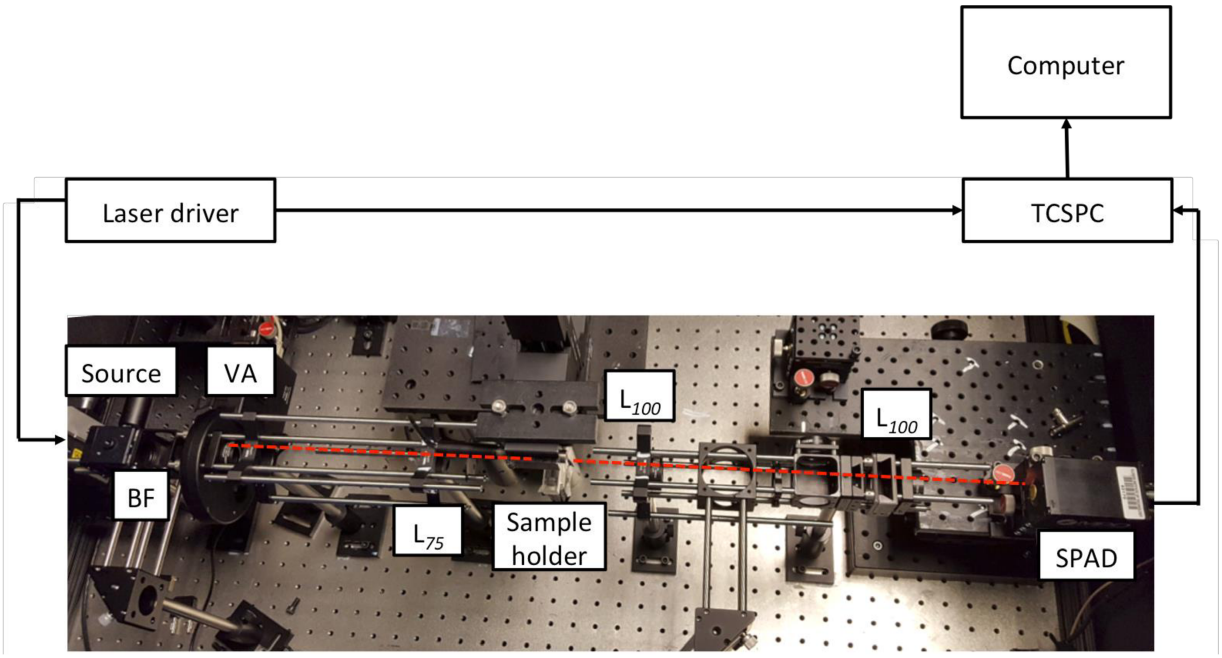

Figure 2. The experimental setup is shown. BF: band pass filter; VA: variable attenuator; L_f: *f* mm focal length lens; SPAD: Single photon avalanche diode; TCSPC: Time correlated single photon counting. The source is the laser head that is controlled by the laser driver module, which also sends the synchronization signal to the TCSPC. The TCSPC takes in the synchronization signal and the detection signal from SPAD and generates and sends the histogram to the computer.

2.2 Simulation of time response of TCSPC

As a laser pulse travels through the tissue it gets spread in time domain and generates the temporal pulse spread function (TPSF). This TPSF can be mathematically generated using the solution to the diffusion approximation of the radiative transport equation (assuming an instantaneous source pulse)[15]. An example TPSF is shown in **Fig. 3a** corresponding to a 6 mm thick tissue sample with absorption and reduced scattering coefficient of 0.04 and 1 mm^{-1}. However, as the temporal resolution of the detector is known to be 1 ± 12 ps, the uncertainty in the detector will spread the TPSF further in time domain before it gets binned in the TCSPC. To understand how the detector uncertainty affects the temporal pulse spread function (TPSF) a simulation study was performed. **Fig. 3b** shows a simulated detector response function (DRF) having a Gaussian profile with a 12 ps standard deviation. The TPSF is now sampled at 100 fs interval (**Fig. 3c**) and each sample is then convolved with the DRF (**Fig. 3d**) to simulate what happens at the detector when it gets detected before it gets binned by the TCSPC. Thus the signal which is fed to the TCSPC is DRF(t) * TPSF(t), '*' denotes convolution. The TCSPC then bins this detected signal in the histogram with either 1,2 or 4 ps bin width that then determines the temporal resolution of the histogram (**Fig. 3e**). **Fig. 3e** shows how the spreading due to the DRF gives more weight on the earlier intervals compared to the later ones in one bin. Any bin will have higher weightage on the earlier photons compared to the later ones due to the spreading by the DRF. However, it should also be noted that as the TPSF gets spread out due to the DRF even though we might observe higher contribution from earlier bins but the signal in those bins will also be low.

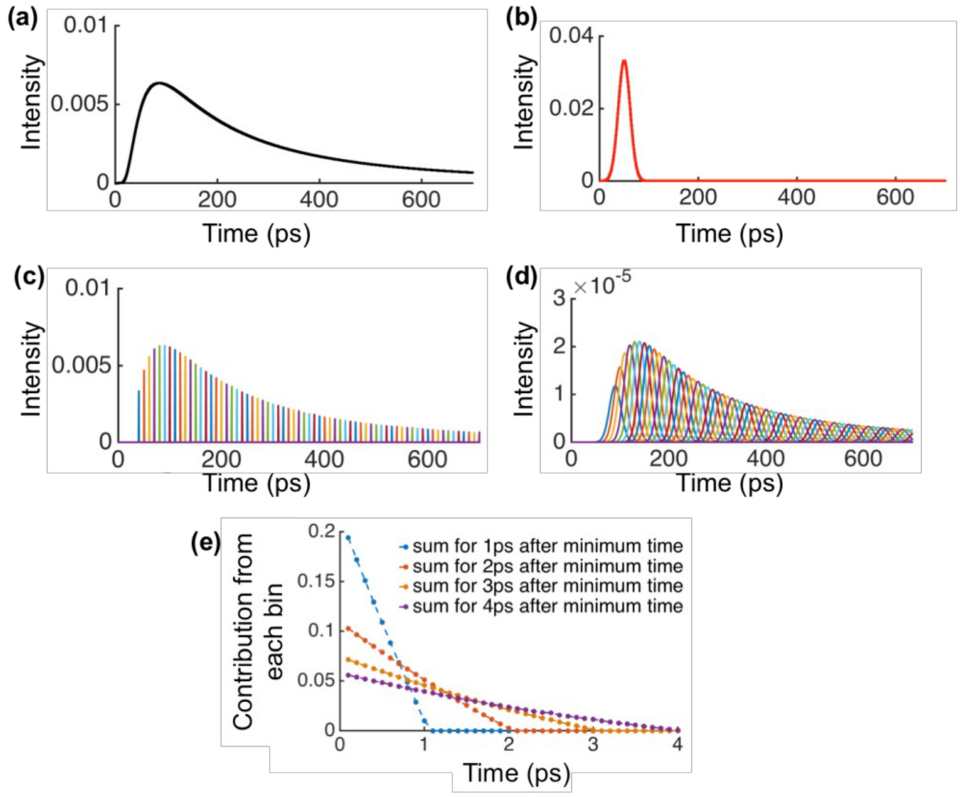

Figure 3.Simulation study showing the spread of the temporal pulse spread function as it gets binned in the TCSPC. (a) The temporal pulse spread function for a 6 mm thick tissue with absorption and reduced scattering coefficient of 0.04 and 1 mm^{-1}; (b) Simulated detector response function (DRF) of the system; (c) Example samples of the sampled TPSF at 100fs (example intervals are shown); (d) The convolution of those intervals (shown in (c)) with the DRF of the detector; (e) The contribution from each interval as they get binned in the TCSPC. Sum for t ps after minimum time denotes the window of bin width that is considered for histogramming in TCSPC.

2.3 Monte Carlo Simulation

Monte Carlo method is a powerful tool to get the same information as the radiative transport equation (but without any diffusion approximation and therefore gives more accurate result) to simulate photon transport in tissue. In this method a stochastic model is used where random sampling is done to determine the solution to a problem[16 , 17]. Monte Carlo modeling generates the path of photons as they get scattered or absorbed inside the tissue. The Monte Carlo simulation was based on a code[18] which was modified with the following changes - 1) a detector of a particular radius was added; 2) if the photons hit the boundary outside the detector then it was made to reflect back depending on Fresnel ratio; 3) the detector was made to accept only those photons which reached within certain restriction (in time) and finally 4) a Gaussian source of a particular radius was simulated with defined radius. **Fig. 4** gives the flowchart that was followed to propagate the photons inside the tissue. Once a photon is initialized with a *weight*=1 a random step *s* is computed, where

$$s = -\frac{\ln(\xi)}{\mu_t} \tag{1}$$

where ξ is a random number between 0 and 1 and μ_t is the total attenuation coefficient ($\mu_t = \mu_a + \mu_s$) ; μ_a being the absorption coefficient and μ_s is the scattering coefficient. For a Gaussian source it is then checked if it is the first interaction point. If it is, then at first the waist (w) and radius of curvature (R) at the interaction point is calculated[19]:

$$w = w_0 * \left[\sqrt{1 + \left(\frac{\lambda(d-zf)}{\pi {w_0}^2}\right)^2}\right] \tag{2}$$

$$R = (d - zf) * \left[1 + \left(\frac{\pi {w_0}^2}{\lambda(d-zf)}\right)^2\right] \tag{3}$$

where, w_0 is the waist at the focal point of the Gaussian beam d is the depth inside tissue and zf is the depth at which the beam focuses; then the position of the photon is:

$$x = w\sqrt{2ln\xi_2}\cos(2\pi\beta) \tag{4}$$

$$y = w\sqrt{2ln\xi_2}\sin(2\pi\beta) \tag{6}$$

$$z = s \tag{7}$$

where $\beta\ and\ \xi_2$ are randomly selected between 0 and 1. Finally, the following relation computes the direction of propagation of the photon:

$$f = x^2 + y^2 + z^2 - R^2 \tag{8}$$

$$\frac{\nabla(f)}{\|f\|} = u\,\hat{\imath} + v\,\hat{\jmath} + w\,\hat{k} \tag{9}$$

where ∇ denotes the gradient operator and u,v,w are the corresponding cosine of the angles with their respective axes. If it is not the first interaction point, the photon is propagated by s where it may be scattered to a new direction, absorbed at that interaction point, $weight = weight\left[1 - \frac{\mu_a}{\mu_t}\right]$, propagated undisturbed, internally reflected or transmitted outside the tissue. At each interaction point the weight absorbed is stored and the remainder of the weight is propagated. If the s is such that the photon is propagated outside the tissue then at first it is checked if it is within the detector radius, if yes then it is retracted back to the tissue surface and if the conditions (restrictions like accepting photons only within a 1 ps window from the expected arrival time) are met then the detected photon profile is updated. If the photon reaches the detector the *weight* is made equal to 0 (absorbed by the detector), if not then either the photon is internally reflected or a portion of the *weight* is reflected back inside the tissue and a portion is transmitted depending on Fresnel ratio. The photon is moved repeatedly by this process until the photon is absorbed (*weight* = 0) either at the detector or in the tissue. This process is repeated till the desired number of photons is reached. As the number of photons becomes infinity the absorption profile will be more precise. Since Monte Carlo is a statistical procedure, large number of photons is desired to be propagated to achieve the desired precision and resolution, however the larger the number, the method gets more computation intensive.

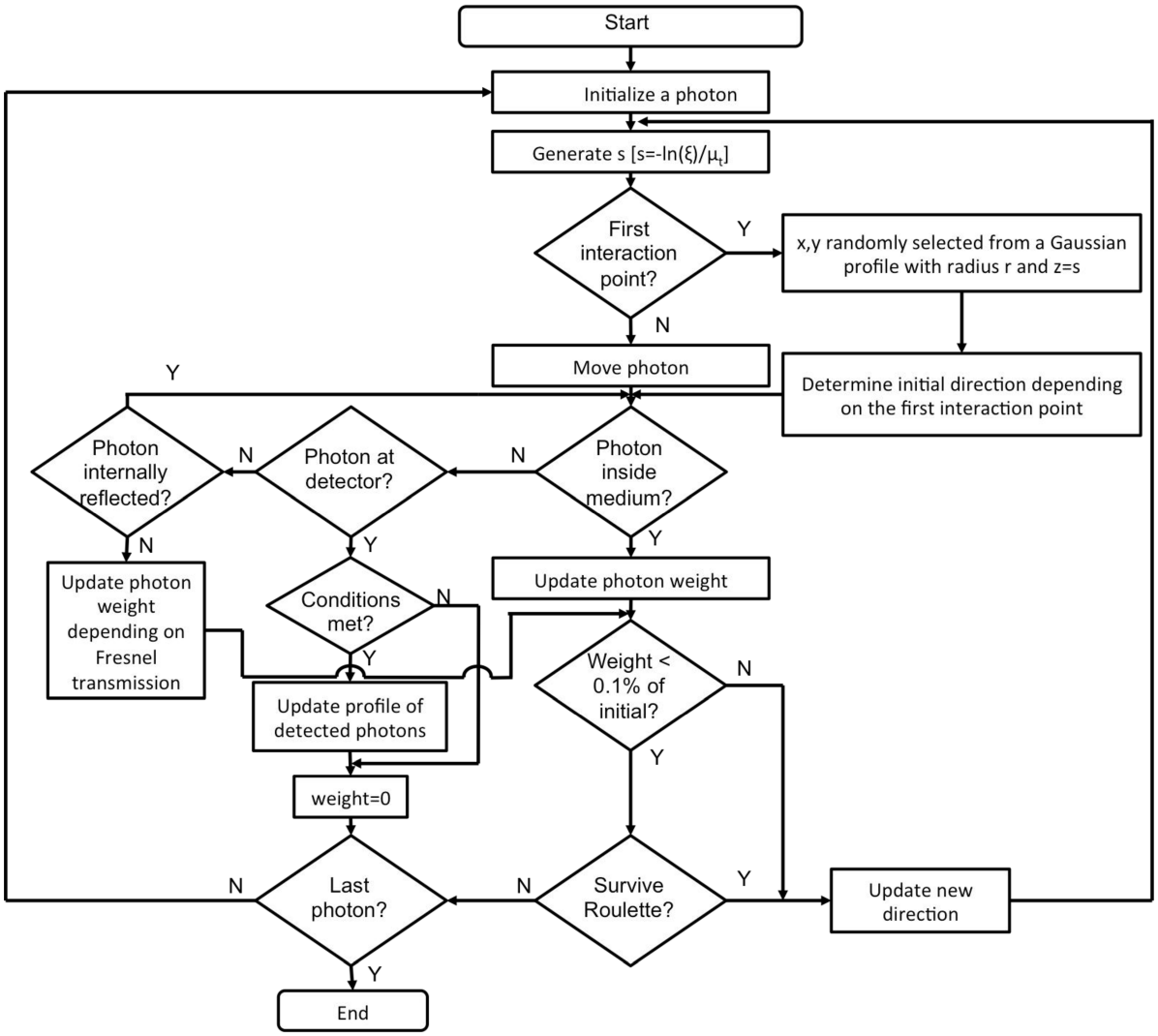

Figure 4. Flowchart of the Monte Carlo simulation used for the study. Once the photon is initialized a random step size determines its interaction point. If it is the first interaction point of the photon, the position and angle of the photon is determined at that point depending on the Gaussian profile of the incident laser beam at that interaction depth. If it is not the first interaction point the photon is moved by the step size. After moving, if it is outside the tissue boundary then it is first checked if it has reached the detector, if yes then the detected profile is updated if the condition for restrictions are met and the weight of the photon is made 0. If it is outside the boundary and is not within the detector radius then the angle is checked for total internal reflection, if it less than the critical angle then the photon is reflected back, however if it is more than the critical angle a part of the photon weight is reflected back and a part is transmitted depending on the Fresnel transmission. However, after moving, if it is inside the medium a part of the photon weight is absorbed at that interaction depth and the photon weight is updated. Next, it is checked if the weight of the photon is above a minimum, if it is then it continues to propagate with the new direction if not then it is checked if it survives Roulette, if it survives it continues to propagate. If not or if the photon reaches the detector in either case it is checked if it is the last photon. If it is less than the desired number of photons another new photon is launched and the process continues. The process stops when the desired number of photons is reached.

2.4 Results and discussion

Fig.5a shows the sensitivity profiles of the weight absorbed that were generated using the above Monte Carlo simulation for a tissue of 2 mm thickness with an absorption coefficient and reduced scattering coefficient of 0.04 mm^{-1} and 1 mm^{-1} respectively (with an anisotropy factor of 0.9). While **Fig.5a-i** depicts a typical sensitivity profile, **Fig.5a-ii** shows the change in the sensitivity profile when only those photons are accepted which is restricted at the detector within a 1 ps

window from the theoretical arrival time (i.e. 10 ps where the refractive index of medium is 1.5). The restriction made the process longer and while only 1.4x10^8 photons were launched for the no restriction case, 5x10^8 photons were launched to observe 15000 photons at the detector in the respective cases. A comparison between the sensitivity profiles shows the rejection of most of the scattered photons while only the straighter ones are accepted at the detector when only those photons are accepted which come within the first picosecond. **Fig. 5b** shows that even at 2 mm thick tissue, a 1ps restriction not only rejects most of the scattered photons but also narrows the FWHM 0.85 times ($FWHM_{no\_restriction}$=297 μm and $FWHM_{1ps\_restriction}$=251 μm), which is directly related to the resolution of the image formed. It is believed that thicker the sample more improvement in FWM reduction will be observed by restricting the acceptance window to 1 ps.

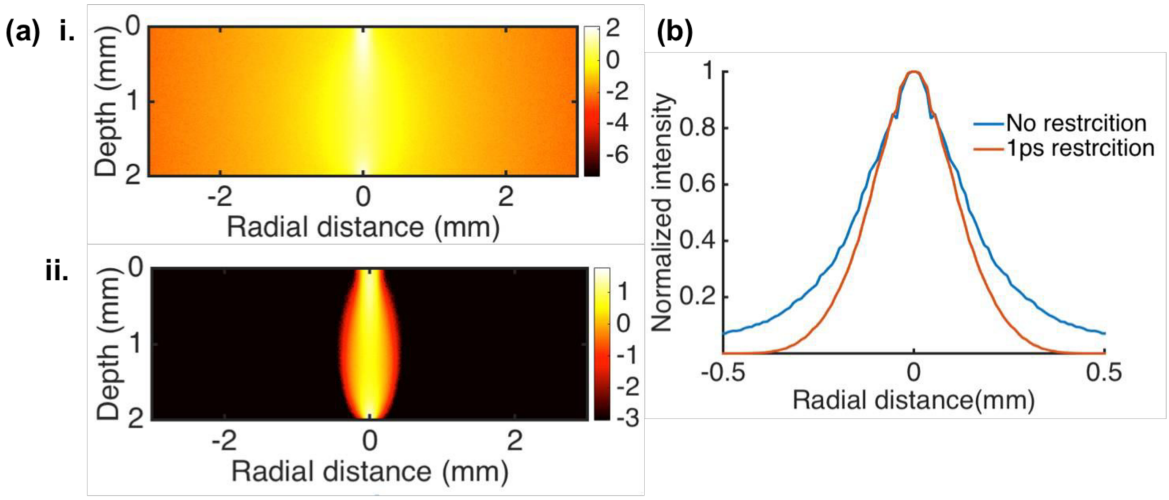

Figure 5. (a-i) Simulated sensitivity functions for a 2 mm thick tissue with absorption coefficient and reduced scattering coefficient of 0.04 mm^{-1} and 1 mm^{-1} respectively (anisotropy factor = 0.9). This corresponds to a 50 μm Gaussian source and 50 μm detector radius placed at opposite ends of the sample. (a-ii) The same sensitivity function when a 1 ps restriction is applied on the detector. The photons coming at the detector outside a 1ps window from the expected arrival time are rejected. (b) The normalized intensity profiles of the sensitivity functions are provided for the above two cases averaged over few rows at the center (1 ± 0.15 mm). FWHM for the no restricted case and the 1ps restriction case was 297 μm and 251 μm respectively.

The results from the unrestricted Monte Carlo simulation must be convolved with the DRF and then restricted to 1 ps bin to simulate what is observed experimentally. While, the enhancement in the early photon imaging by saturating the detector is already shown[2], it is also observed that with increased laser power the background signal (which constitutes mostly of the afterpulsing signal) might get saturated. Since the afterpulsing signal is directly related to the number of photons detected, at higher laser power as the number of photons detected gets saturated, even though more early photons are detected masking more and more of the late arriving photons with higher power, the number of afterpulsing photons also saturates. **Fig. 6** shows the TPSF through a 4mm thick tissue with absorption coefficient and reduced scattering coefficient of 0.04 mm^{-1} and 1 mm^{-1} in both conventional and saturated mode of the detector when the same amount of energy ($1.68x10^{-3}$ J) is delivered to the sample but the conventional mode is performed at a power which will not saturate the detector (0.01mW of laser power over 200 s of acquisition) while in the saturated mode higher laser power is used that will induce dead time in the detector but in turn requires shorter acquisition time to reach the same energy (10mW of power over 0.2 s of acquisition). While similar early photon signal (denoted by the green dot dashed line in **Fig. 6**) is observed in both the cases, the conventional mode had much higher background signal (denoted by the dashed black line) compared to the saturated mode due to higher number of afterpulsed photons. The signal to background ratio was computed to be 7 and 544 for the conventional mode and the saturated mode respectively, showing a 77 times improvement. It should also be noted here that the signal obtained from the conventional mode took 1000 times longer than the same amount of signal obtained from the saturated mode.

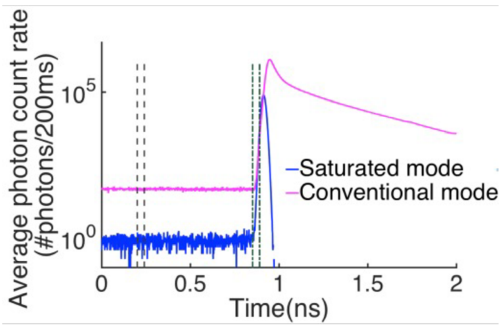

Figure 6. Energy matched TPSFs in conventional mode and saturated mode respectively. While the black dashed line marks the background region, the early photons are selected from the green dot dashed line. The pink data corresponds to a 0.01mW of laser power over 200 s of acquisition and the blue data corresponds to a saturated detector with 10mW of power (deadtime inducing power) over 0.2 s of acquisition.

3. CONCLUSION

A novel approach is discussed in optical projection imaging to achieve high-resolution images through thick tissue samples (< 100 μm resolution through a 4 mm tissue sample), by utilizing 'dead-time' effect in single photon detector. Detector saturation not only can help enhance collection of rare early photons but can also significantly reduce the background noise owing to the saturation of the afterpulsing signal which can further enhance the signal to background ratio. With a relatively modest power pulsed femtosecond laser (12 mW), the early photon detection rates were 3 orders of magnitude (reducing needed acquisition time 1000 times), more than that achievable for detection in conventional mode and signal-to-background improvements of over 70-times were observed.

REFERENCES

[1] L. Fieramonti, A. Bassi, E. A. Foglia *et al.*, "Time-gated optical projection tomography allows visualization of adult zebrafish internal structures," PLoS One, 7(11), e50744 (2012).

[2] L. Sinha, J. G. Brankov, and K. M. Tichauer, "Enhanced detection of early photons in time-domain optical imaging by running in the "dead-time" regime," Opt Lett, 41(14), 3225-8 (2016).

[3] A. Jemal, F. Bray, M. M. Center *et al.*, "Global cancer statistics," CA Cancer J Clin, 61(2), 69-90 (2011).

[4] D. L. Weaver, "Pathology evaluation of sentinel lymph nodes in breast cancer: protocol recommendations and rationale," Mod Pathol, 23 Suppl 2, S26-32 (2010).

[5] R. Pijpers, P. J. Borgstein, S. Meijer *et al.*, "Sentinel node biopsy in melanoma patients: dynamic lymphoscintigraphy followed by intraoperative gamma probe and vital dye guidance," World J Surg, 21(8), 788-92; discussion 793 (1997).

[6] K. M. Tichauer, K. S. Samkoe, J. R. Gunn *et al.*, "Microscopic lymph node tumor burden quantified by macroscopic dual-tracer molecular imaging," Nat Med, 20(11), 1348-53 (2014).

[7] V. V. Tuchin, "Light scattering study of tissue," Russian academy of science, 167(5), 517-539 (1997).

[8] A. P. Gibson, J. C. Hebden, and S. R. Arridge, "Recent advances in diffuse optical imaging," Phys Med Biol, 50(4), R1-43 (2005).

[9] S. R. Arridge, and J. C. Schotland, "Optical tomography: forward and inverse problems," Inverse Problems, 25(12), (2009).

[10] L. Wang, P. P. Ho, C. Liu *et al.*, "Ballistic 2-d imaging through scattering walls using an ultrafast optical kerr gate," Science, 253(5021), 769-71 (1991).

[11] M. J. Niedre, R. H. de Kleine, E. Aikawa *et al.*, "Early photon tomography allows fluorescence detection of lung carcinomas and disease progression in mice in vivo," Proc Natl Acad Sci U S A, 105(49), 19126-31 (2008).

[12] A. Bassi, D. Brida, C. D'Andrea *et al.*, "Time-gated optical projection tomography," Opt Lett, 35(16), 2732-4 (2010).

[13] W. Tan, Z. Zhou, A. Lin *et al.*, "High contrast ballistic imaging using femtosecond optical Kerr gate of tellurite glass," Opt Express, 21(6), 7740-7 (2013).

[14] F. Vasefi, B. Kaminska, G. H. Chapman *et al.*, "Image contrast enhancement in angular domain optical imaging of turbid media," Opt Express, 16(26), 21492-504 (2008).
[15] M. S. Patterson, B. Chance, and B. C. Wilson, "Time resolved reflectance and transmittance for the non-invasive measurement of tissue optical properties," Appl Opt, 28(12), 2331-6 (1989).
[16] M. K. S. A. Prahl, S. L. Jacques∗, A. J. Welch, "A Monte Carlo Model of Light Propagation in Tissue," SPIE Institute Series, IS 5, 102-111 (1989).
[17] Q. Fang, and D. A. Boas, "Monte Carlo simulation of photon migration in 3D turbid media accelerated by graphics processing units," Opt Express, 17(22), 20178-90 (2009).
[18] S. Jacques, [A Monte Carlo subroutine in ANSI-standard C].
[19] H. Kogelnik, and T. Li, "Laser beams and resonators," Appl Opt, 5(10), 1550-67 (1966).